Corrosion Science 53 (2011) 1794–1805

Contents lists available at ScienceDirect

Corrosion Science

journal homepage: www.elsevier.com/locate/corsci

Shear performance of reinforced concrete beams with corroded stirrups in chloride environment

Jin Xia [a,*], Wei-liang Jin [a], Long-yuan Li [b]

[a] Institute of Structural Engineering, Zhejiang University, Hangzhou 310058, PR China
[b] School of Civil Engineering, University of Birmingham, Birmingham B15 2TT, UK

ARTICLE INFO

Article history:
Received 27 October 2010
Accepted 29 January 2011
Available online 4 February 2011

Keywords:
A. Concrete
B. Electrochemical calculation
B. Weight loss
C. Pitting corrosion

ABSTRACT

Experiments were conducted for the investigation of the influence of reinforcing steel corrosion on the shear capacity of reinforced concrete beams. The shear performance of RC beams with different corrosion levels in both longitudinal reinforcing steel bars and stirrups was examined. Relationships of corrosion-induced crack widths in concrete cover with the corrosion level of the reinforcing steel bars were obtained. Engineering approaches were developed to predict the residual shear strength of the corroded beams.

1. Introduction

Reinforced concrete (RC) structures, exposed to environments where de-icing salts or coastal/marine conditions are encountered, often exhibit premature deterioration and require unplanned maintenance. The major cause of these problems is the chloride-induced corrosion of reinforcing steel which, because of the substantial volume increase that accompanies the transformation of iron to rust, can lead to cracking and spalling of the concrete cover. In addition, the corrosion of reinforcing steel bars can also cause a weakening of the bond and anchorage between concrete and reinforcement, which can reduce the shear capacity of RC beams and affects the serviceability and ultimate strength of concrete elements in RC structures.

Despite a large body of literature on the corrosion of reinforcing steel induced by chlorides [1–4] and corresponding influence of reinforcing steel corrosion on the flexural capacity of RC beams [5,6] there are few works that have dealt with the reduction in shear capacity of RC beams due to the corrosion of stirrups in RC beams [7]. Stirrups play an important role in RC beams. They can directly sustain shear force and indirectly enhance the load-carrying ability of other elements in the RC beam. The adequate use of stirrups in a RC member can control the horizontal splitting cracks at the level of the longitudinal reinforcement, which can increase the strength of the dowel action and thereby enhance the shear capacity of the member. Besides this, the stirrups can also limit crack propagation and crack widths. Note that, stirrups, in most RC beams, are nearer to the concrete surface than the longitudinal steel bars. Therefore, stirrups would be first attacked by chlorides in a chloride environment. Moreover, stirrups are generally made of small diameter steel bars and therefore if they are corroded, the stirrups will be quick to loss their load-bearing ability [8].

The shear strength of RC beams with a part of the longitudinal reinforcement exposed over varying portions of the span was evaluated by Cairns [9], who used a method of analysis based on existing semi-empirical rules in BS 8110. His study suggested that the shear strength is increased when reinforcement is exposed in all but the most lightly reinforced sections. Rodriguez et al. [10] conducted an experimental study on corroded RC beams in which reinforcement was corroded by means of adding calcium chloride to the mixing water and applying a constant current density of about 1 A/m^2. The results showed that the corrosion increases both deflections and crack widths at the service load, reduces the strength at the ultimate load, and modifies the type of failure from bending for sound tested beams to shear for deteriorated beams. Yan et al. [11] investigated the shear performance of RC beams with different mix proportions under different wetting–drying cycle conditions. The beams were exposed to artificially imitating sea water to simulate the sea water wave splash. Xu and Niu [12] investigated the effects of corrosion rate of stirrups on the deformation, crack forming and development, bearing capacity and failure mechanism of RC beams by using experimental methods. They found that, the corrosion of stirrups reduces the constraint of stirrups to surrounding concrete; the grip action of aggregates at both sides of the crack is deteriorated as the diagonal crack develops rapidly; and the stirrup corrosion has significant influence on the

* Corresponding author. Tel.: +86 571 88208733x610; fax: +86 571 88208733x601.
E-mail address: xiajin2008@gmail.com (J. Xia).

0010-938X/$ - see front matter © 2011 Elsevier Ltd. All rights reserved.
doi:10.1016/j.corsci.2011.01.058

shear bearing capacity of the beam. Higgins and Farrow [7] investigated the shear performance of corroded RC beams with three different cross-section types (rectangle, T and upturned T-cross sections). It was showed that all corroded beams have reduced shear capacity and reduced overall deformation at the failure point. Recently, Zhao et al. [13] carried out an extensive theoretical and experimental study on the effect of stirrup corrosion on the shear capacity of RC beams. They found that the shear strength of RC beams increases at the early stages of stirrup corrosion and the loss in shear strength actually starts when the corrosion of the stirrups approximately exceeds 10% of its threshold level.

Most of existing experiments mentioned above used either chloride pre-blending or a constant current method to accelerate the corrosion of internal reinforcing steel bars in RC beams. As a consequence of this, the corrosion of the steel bars was developed uniformly along its whole surface [14,15]. In the real case, however, the corrosion of the steel bars mainly occurs on one side of its surface, which is facing the concrete cover. In order to accurately predict the effects of the localised reinforcing steel corrosion or pitting corrosion on the development of tensile stresses in its surrounding concrete and the propagation of cracks in its concrete cover, it is necessary to simulate the corrosion distribution according to the corrosion pattern happened in a natural environment [16].

In this paper, an experimental study is presented on the influence of reinforcing steel corrosion on the shear capacity of conventionally RC beams. The experimental programme involved an electrochemical process to accelerate the migration of chlorides from an external electrolyte into the tested beams, a wetting–drying cycle process with a controlled current to speed up the corrosion of the reinforcing steel bars in the tested beams, and a strength test to determine the shear capacity of the tested beams. The shear performance of RC beams with different corrosion levels in both longitudinal reinforcing steel bars and stirrups was examined. Relationships of corrosion-induced crack widths in concrete cover with the corrosion level of the reinforcing steel bars were obtained. Engineering approaches were developed to predict the residual shear strength of the corroded beams.

2. Experimental programme

The experiments involved an electrochemical process with a controlled voltage difference between an anode embedded in the tested beam and a cathode placed in an external electrolyte to accelerate the migration of chlorides from the external electrolyte into the beam, a wetting–drying cycle process with a controlled current to speed up the corrosion of the reinforcing steel bars in the beam, and a strength test to determine the shear capacity of the beam. A total of 18 RC beams in three different groups were tested in the present experimental programme, which includes 15 corroded beams and three un-corroded beams. The following are the details of the beam specimens, set-up and undertaking of the experiments.

2.1. Specimen details

The concrete used for making the RC beams is the ordinary Portland cement with a compressive strength of 42.5 MPa (cylinder specimen test) and the coarse aggregate with 16 mm maximum size gravel (see Table 1 for the details). The designed slump constant was 70 mm. In addition, three $150 \times 150 \times 150$ mm cubic specimens were also casted in order to obtain the compressive strength of the mixed concrete. The 28 day average compressive strength of the three casted cubic specimens was found to be 25.93 MPa.

Table 1
Proportion of concrete mix.

w/c Ratio	Water (kg/m^3)	Cement (kg/m^3)	Fine aggregate (kg/m^3)	Coarse aggregate (kg/m^3)
0.53	220	412.5	641.2	1046.1

Table 2
Characteristics of the reinforcing bars.

Rebar grade	Nominal diameter (mm)	Actual cross-section area (mm^2)	Yield strength (N/mm^2)	Ultimate strength (N/mm^2)	Elasticity modulus (N/mm^2)	Elongation (%)
ϕ	6	33.59	321.80	441.11	1.96×10^5	34.44
ϕ	8	46.00	463.87	515.70	1.98×105	25.00
ϕ	10	90.04	319.60	461.86	2.07×105	32.00
⌀	20	291.79	380.05	582.10	1.86×10^5	32.00
⌀	20	306.80	570.83	715.88	2.03×10^5	24.00

All reinforcing steel bars used in the RC beams were the hot rolled steel bars. They were the smooth HPB235 (ϕ) bar, the deformed HRB335 (⌀) bar, and the deformed HRB500 (⌀) bar, respectively. The dimensions and material properties of the reinforcing steel bars are given in Table 2. Note that the diameter shown in Table 2 is the nominal diameter of the bar provided by the manufacturer, whereas the cross-section area of the bar is the actual area which was calculated from the weighted mass divided by the steel density and the measured length. The yield strength, ultimate strength and the modulus of elasticity of the bar were obtained by using standard tensile tests. The elongation was the tensile stretch of the bar in a length of five times its diameter near the rupture area.

In order to increase the flexural capacity of the beam, two longitudinal steel bars were placed in the bottom layer of the beam. Fig. 1 shows the details of the reinforcement arranged in the tested beams. For each of the three tested beam groups, six RC beams were first casted, then corroded, followed by a mechanical loading test. All of the beams have the same dimensions, which are 230 mm in depth, 120 mm in width and 1200 mm in length. The beams were represented by a letter followed by a numerical number. The letter corresponds to the details of the reinforcing steel bars, in which letter 'A' represents the case where the beam has two ⌀20 longitudinal reinforcing steel bars in the bottom layer,

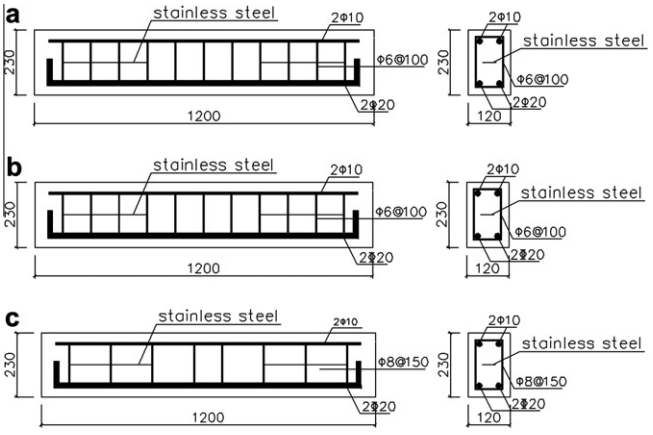

Fig. 1. Details of the beam specimen (units: mm). (a) Type A; (b) Type B and (c) Type C.

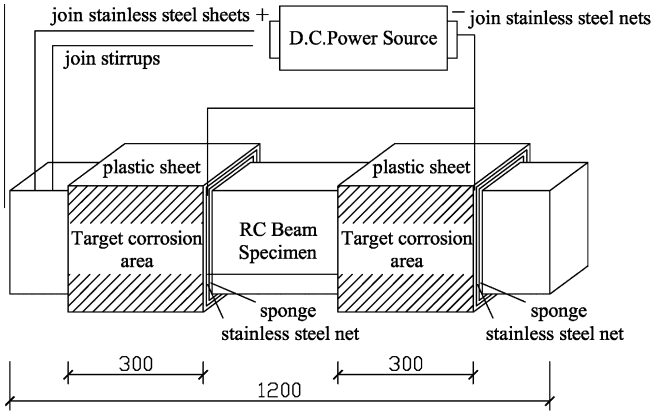

Fig. 2. Schematic representation of accelerated corrosion test setup (units: mm).

11 stirrups (spacing 100 mm) of 6 mm diameter steel bars; letter 'B′ represents the case where the beam has two ⌀20 longitudinal reinforcing steel bars in the bottom layer, 11 stirrups (spacing 100 mm) of 6 mm diameter steel bars; and letter 'C′ represents the case where the beam has two ⌀20 longitudinal reinforcing steel bars in the bottom layer, 8 stirrups (spacing 150 mm) of 8 mm diameter steel bars. The numerical number used is to indicate the corrosion damage level, in which number '0′ stands for no corrosion and number '5′ stands for the heaviest corrosion. For example, the beam B-3 means that the beam has two ⌀20 longitudinal reinforcing steel bars in the bottom layer, 11 stirrups (spacing 100 mm) of 6 mm diameter steel bars, with a corrosion damage level 3.

All of the tested beams have two ϕ10 longitudinal reinforcing steel bars in the top layer, which were anchored with the two longitudinal bars in the bottom layer using a standard hook length of 100 mm to prevent anchorage failures, a clear concrete cover of 30 mm, and two pieces of 30 × 300 × 0.2 mm stainless steel sheets located in the middle layer of the shear zones near the beam ends. The stainless steel sheets were used purely for the purpose of electro-migration process in which they were acting as an anode for migrating chloride ions into the beam. Owing to the relatively small size and the position where they were located, the two steel sheets would have very little influence on the strength of the beam.

Table 3
Summary of experimental responses.

Beam designation	Galvanizing time t_2 (days)	$\eta_{average,target}$ (%)	$\eta_{average}$ (%)	$w_{c,average}$ (mm)	$w_{c,max}$ (mm)	Ultimate shear force V_u (kN)
A-0	0.00	0	0.00	0.00	0.00	119.5
A-1	23.93	10	10.68	0.06	0.08	126.4
A-2	49.23	20	27.01	0.08	0.12	112.0
A-3	76.16	30	37.13	0.12	0.20	112.5
A-4	105.10	40	42.54	0.12	0.40	105.4
A-5	136.57	50	54.15	0.19	0.48	85.2
B-0	0.00	0	0.00	0.00	0.00	135.6
B-1	23.93	10	12.94	0.04	0.04	124.0
B-2	49.23	20	21.75	0.10	0.12	123.3
B-3	76.16	30	29.23	0.14	0.40	124.0
B-4	105.10	40	41.48	0.13	0.40	119.4
B-5	136.57	50	51.42	0.18	0.44	100.3
C-0	0.00	0	0.00	0.00	0.00	138.2
C-1	31.48	10	6.53	0.08	0.08	133.9
C-2	64.76	20	11.73	0.13	0.24	129.0
C-3	100.19	30	19.54	0.14	0.24	128.1
C-4	138.26	40	25.74	0.16	0.36	131.5
C-5	179.66	50	32.38	0.19	0.68	127.0

All of the tested beams were casted from one batch of concrete, wet cured for a period of 7 days, and then permitted to dry cure for

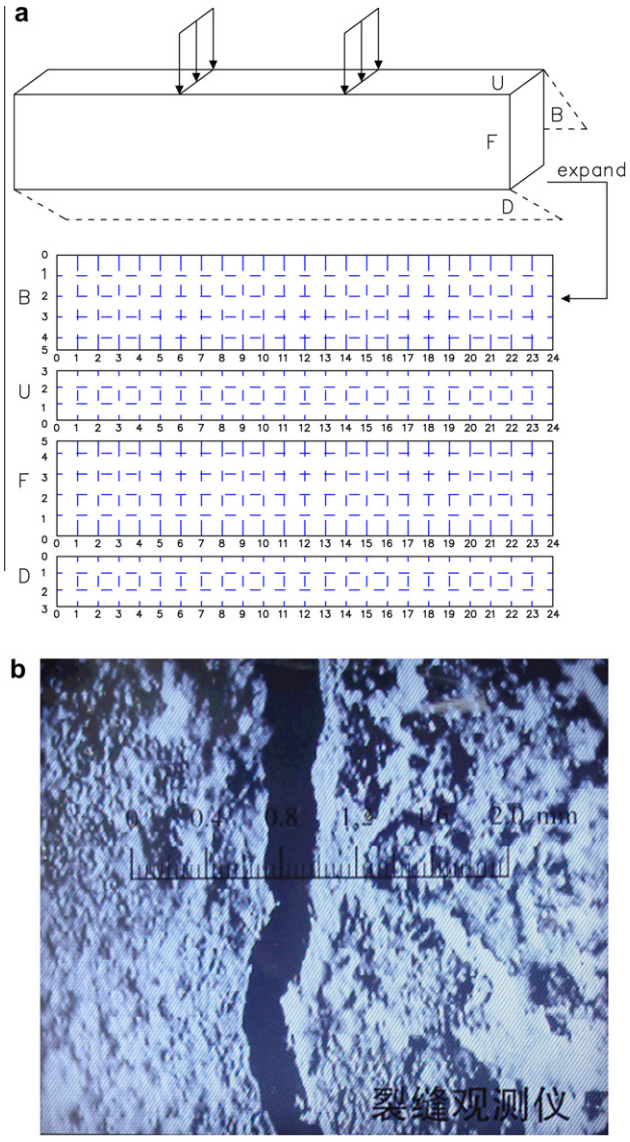

Fig. 3. Measurement of corrosion-induced cracks in concrete. (a) Measurement gird on the beam surfaces and (b) crack width measurement.

a further period of at least 28 days to achieve the required design strength. After curing, an accelerated corrosion process was applied.

2.2. Accelerated corrosion tests

Fig. 2 shows a schematic representation of the test setup for the accelerated corrosion. Since the targeted corrosion area was the stirrups at the two shear zones near the beam ends, sponge which soaks up NaCl solution was used to keep the concrete in the two targeted areas wet. Two stainless steel nets, each in one area, were attached to the sponge. The outside of the beam was then wrapped with a plastic sheet to keep the moisture in the sponge.

The corrosion procedure can be divided into two phases, namely, the electro-migration phase and the wetting–drying cycle phase. In the electro-migration phase, chloride ions were electro-migrated into concrete cover by means of using an electrochemical method. In order to simulate the realistic chloride ingress in concrete, NaCl solution of concentration 2 mol/L was first put in the sponge to make the concrete moisture more than 24 h. Then, the direction of the current flow was adjusted so that the outside stainless steel nets attached to the sponge became the cathode and the embedded stainless steel sheets served as the anode. Finally, a constant voltage of 30 V was applied between the outside stainless steel nets and the embedded stainless steel sheets using a DC power source. Note that the use of the embedded stainless steel sheets rather than the stirrups or longitudinal steel bars as the anode is purely for achieving a high chloride diffusion profile in a short period. The principle of the chloride migration in concrete has been well addressed in literature (see, for example, [17,18]) and thus is not discussed here further. The electro-migration time used in the electro-migration phase was determined based on the chloride concentration at the reinforcement which reaches to a threshold value, using the following equation [18].

$$t_1 = \frac{RT}{zFED_{nssm}}\left[x_d - 2\sqrt{\frac{RTx_d}{zFE}}\,\mathrm{erf}^{-1}\left(1-\frac{2c_d}{c_0}\right)\right] \quad (1)$$

where t_1 is the electro-migration time during which the electro-migration process was applied, $R = 8.314$ J/(mol K) is the gas constant, $T = 298$ K is the average absolute temperature in the tested beam, $z = 1$ is the charge number, $F = 96480$ J/(V·mol) is the Faraday constant, $E = 260$ V/m is the applied electric field strength, $x_d = 0.024$ m for beam groups A and B or $x_d = 0.022$ m for beam group C is the clear concrete cover thickness, $c_d = 0.4225$ mol/L is the chloride threshold concentration which was calculated based on the threshold mass ratio of chlorides to concrete to initiate corrosion, $c_0 = 2$ mol/L is the concentration of free chlorides in the external electrolyte solution, and D_{nssm} is the non-steady state diffusion coefficient. The non-steady state diffusion coefficient was determined by using separate rapid chloride migration tests [18] in concrete cylinders of a diameter of 100 mm and a thickness of 50 mm. For the present concrete, the non-steady state diffusion coefficient was found to be about $D_{nssm} = 6.67 \times 10^{-12}$ m^2/s. This gives the electro-migration times calculated by using Eq. (1) to be $t_1 = 3.80$ days for beam groups A and B, and $t_1 = 3.47$ days for beam group C, respectively.

Previous experience showed that cracks evolve more rapidly in a dry environment than in a humid environment when an accelerated corrosion process is applied [19]. This is probably due to the

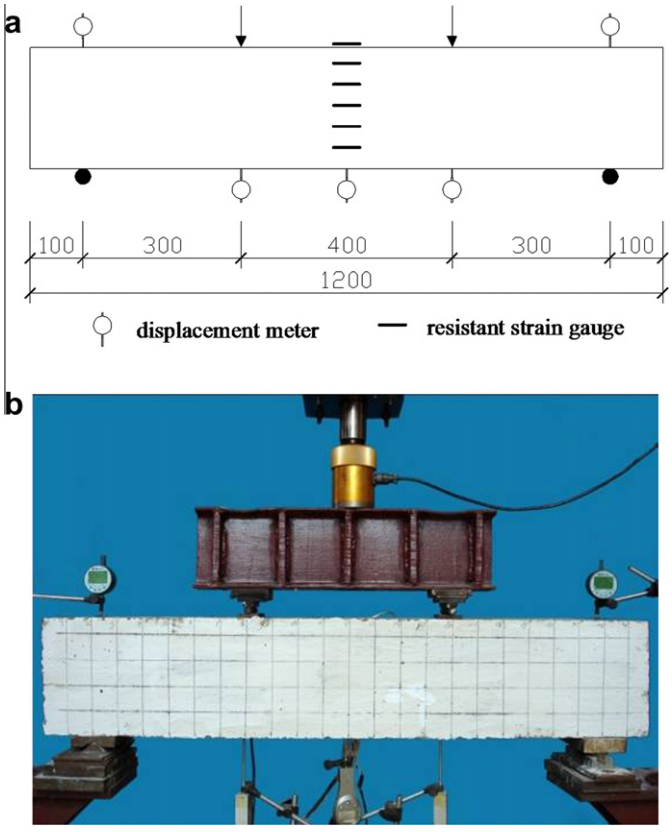

Fig. 4. Loading test arrangement (units: mm). (a) Schematic presentation and (b) on-site loa ding test.

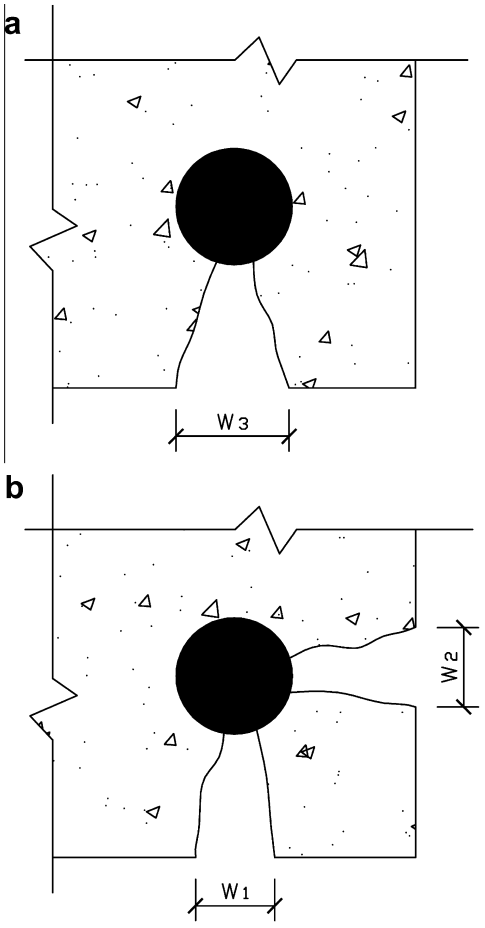

Fig. 5. Two equivalent crack configurations for the same corrosion state. (a) Configuration 1: $w_{c,eq} = w_1 + w_2$ and (b) configuration 2: $w_{c,eq} = w_3$.

transport enhancement of the corrosion products away from the steel–concrete interface in the wet concrete. While in the dry concrete most of the corrosion products stay at the steel–concrete interface. As a consequence of this, pore pressure may increase and additional tensile stresses at the interface may also be developed. This leads to the development of concrete cracks and the propagation of cracks through the concrete cover. Hence, in order to simulate the degradation process happened in real environment, a wetting–drying cycle process was used immediately after the electro-migration process. Each cycle of the wetting–drying process involved 3 days drying followed by 4 days wetting. The drying process was achieved by taking off the plastic sheet to dry the sponge, whereas in the wetting process, the plastic sheet was re-applied to cover over the beam and 5% NaCl solution was put in the sponge to make the concrete moisture. For the purpose of an accelerated corrosion, a current density of 2 A/m^2 was applied during the wetting process through the stirrups (acting as the anode) and the stainless steel nets (acting as the cathode) by using a DC power source. The total galvanizing time was determined by using the following formula [20],

$$t_2 = \frac{\gamma_s Z_{Fe} F \Delta d_s}{M_{Fe} i} \tag{2}$$

where t_2 is the total galvanizing time, γ_s=7850 kg/m^3 is the density of the steel material, Z_{Fe} = 2 is the valence of the iron element, Δd_s is the target corrosion depth which was calculated based on the target

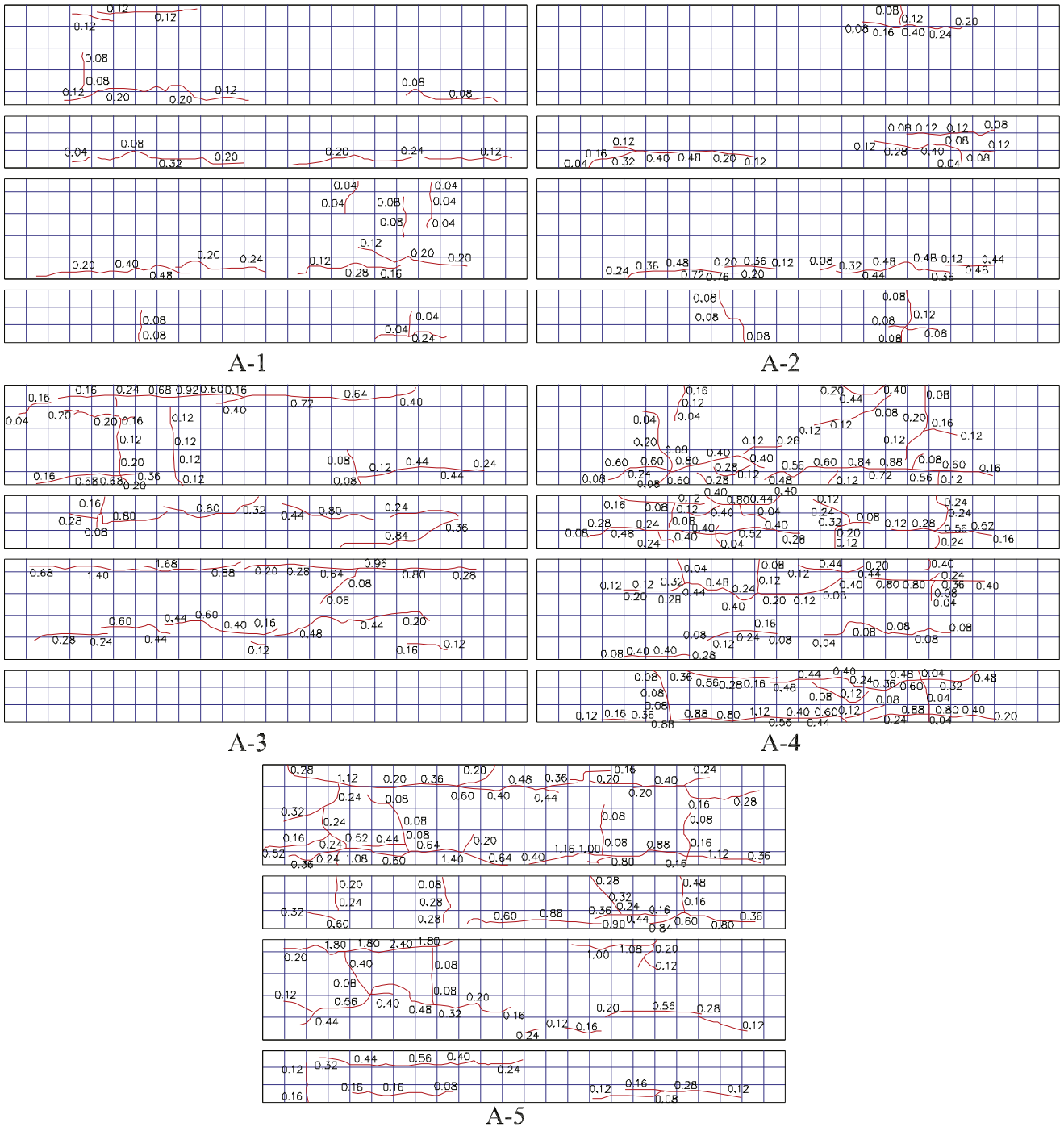

Fig. 6. Corrosion induced crack maps of group A beams (numerical number represents cracking width in mm).

average cross-section loss given in Table 3 for individual beam, $M_{Fe} = 0.056$ kg is the atomic weight of the iron element, and $i = 2$ A/m^2 is the current density applied to the stirrups. Note that the longer the time was applied, the more the chlorides can be transported into the concrete and thus more corrosion will be expected in the steel bars. Hence, different corrosion damage levels can be achieved by using different galvanizing times. Table 3 lists the target corrosion levels and the corresponding galvanizing times calculated for each of tested beams by using Eq. (2).

It should be mentioned here that, the purpose of combining the two accelerated corrosion methods described above is not only for reducing the experimental time but also for matching the corrosion process and behaviour happened in real RC members. Electro-migration is able to simulate the chloride ingress in concrete until the reinforcing steel bars start to corrode. On the other hand, the wetting–drying cycles with controlled current density can reasonably represent the corrosion behaviour of the reinforcing steel bars in real RC members.

2.3. Corrosion-induced cracks in concrete

The surface distribution of corrosion-induced cracks in concrete cover was copied on a paper by putting a piece of soft glass with a grid of 5 × 5 mm on the four surfaces of the tested beam. Crack width was measured using a crack visualize with an accuracy of 0.02 mm at each grid (see Fig. 3).

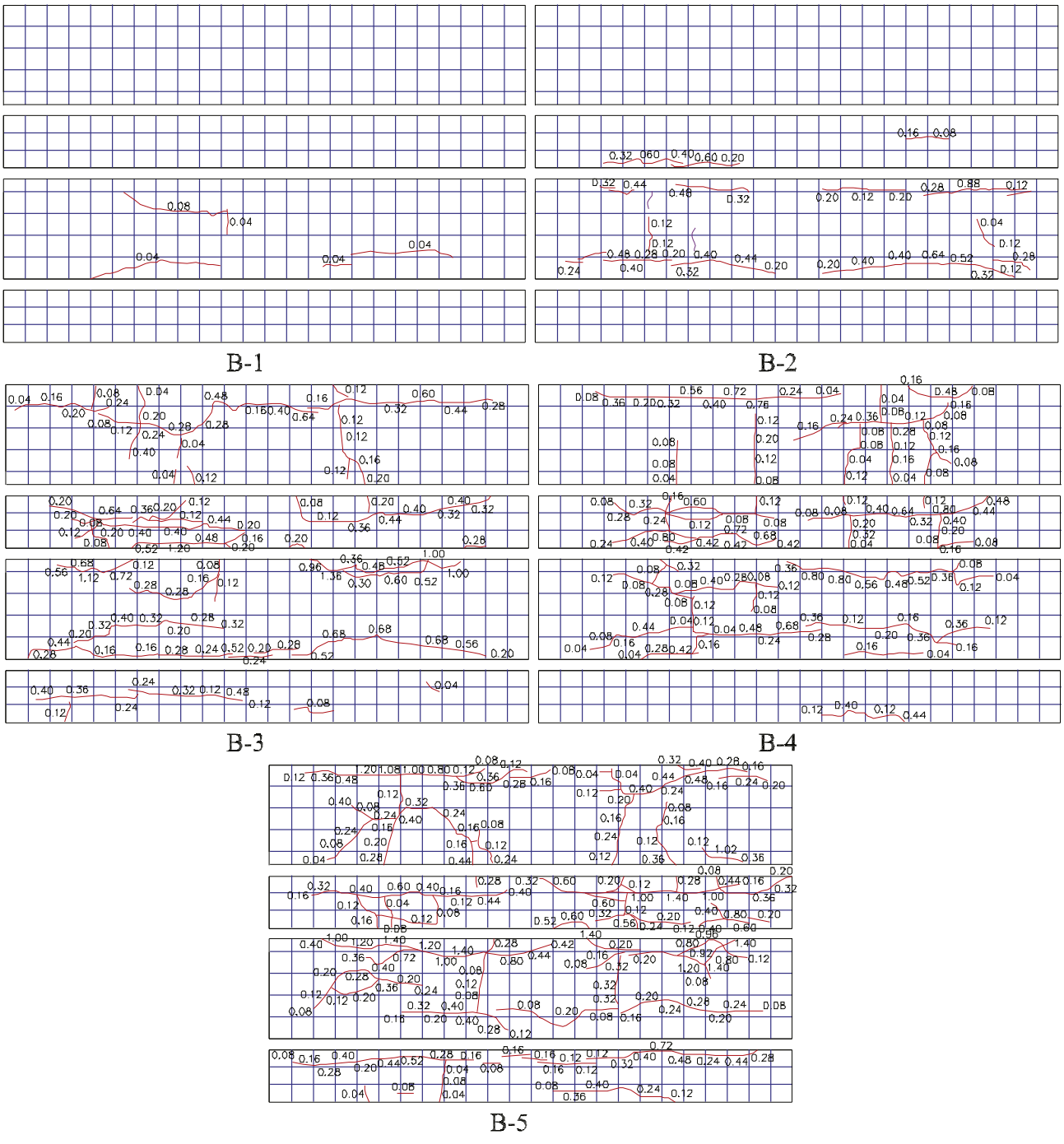

Fig. 7. Corrosion induced crack maps of group B beams (numerical number represents cracking width in mm).

2.4. Loading tests

After they had corroded, each of the beams was tested using a standard four-point loading test equipment (see Fig. 4), where the beam was simply supported at two points near the beam ends and two loading points were symmetrically located in the central part of the beam. The distance between the two loading points is 400 mm. The distance from the support to its near loading point is 300 mm. The beam was loaded with a hydraulic actuator, and a steel element was simply supported on the two load application points of the beam. Loading continued after a maximum load was reached so that the post peak behaviour of the beam could be observed. Five reading meters were used to record displacements, which were placed at the two support points, two loading points and one at the central point of the beam, respectively. Six resistance strain gauges were also used to record the strains of the middle section of the beam from bottom to top. A data collector and the corresponding data processing software were used to collect the data recorded for both the displacements and strains during the loading process. The loading was ended when the beam reached a failure stage.

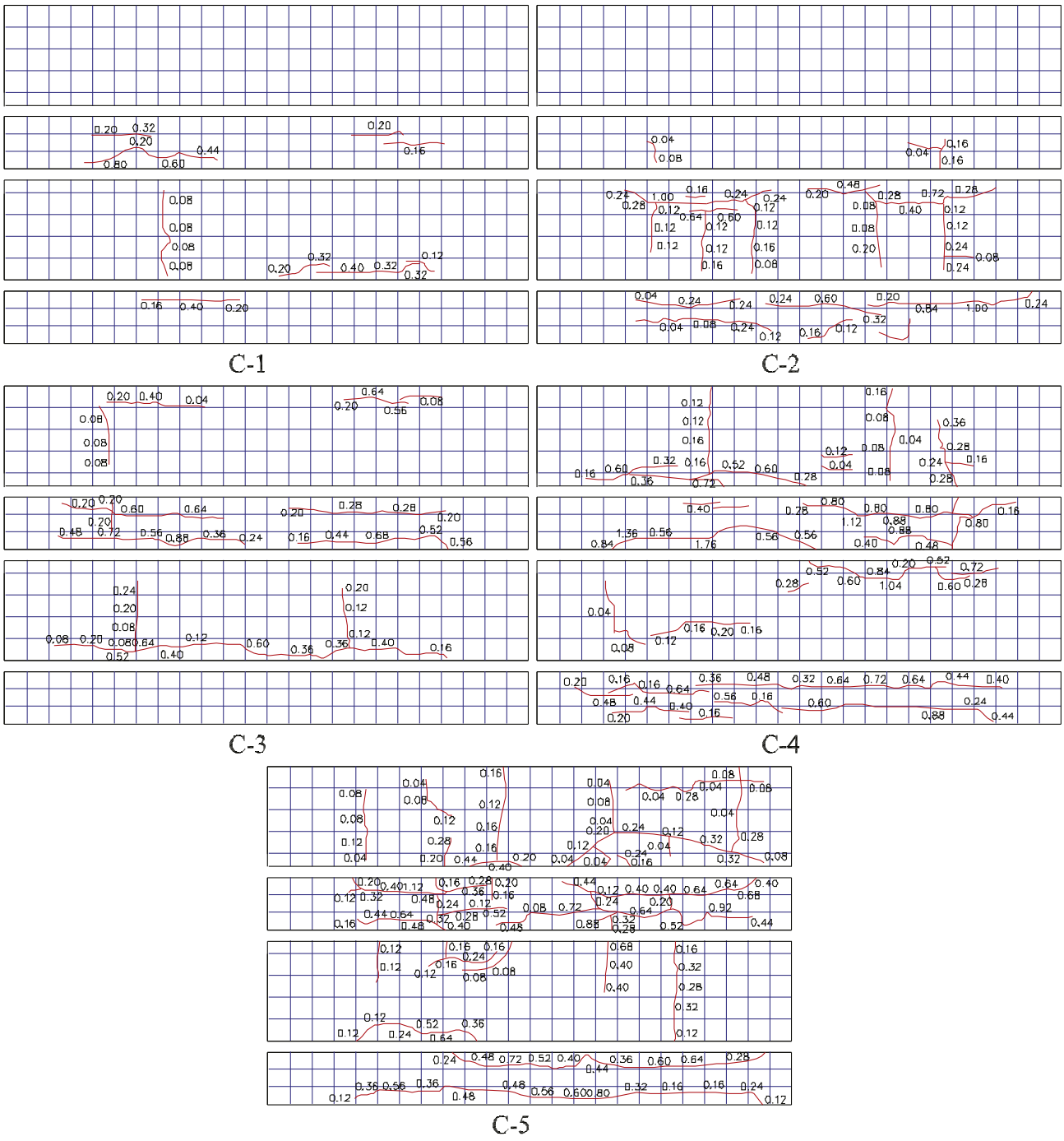

Fig. 8. Corrosion induced crack maps of group C beams (numerical number represents cracking width in mm).

2.5. Corrosion level evaluation

After the loading test of the beam, the stirrup bars were taken out from the beam. The bars were then cleaned and measured according to the method mentioned in ASTM G1-03 [21], from which the average cross-section loss ratios of the stirrup bars $\eta_{average}$ were calculated by using the weight ratios between the corroded and un-corroded bars. The obtained results are given in Table 3.

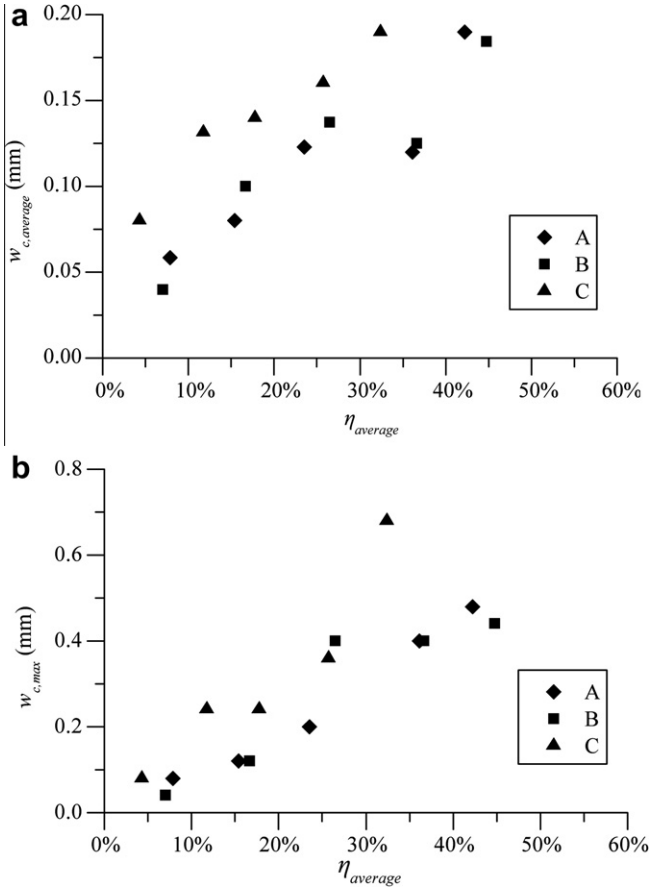

Fig. 9. The relationships between the corrosion-induced crack widths and average cross-section loss ratio. (a) $\eta_{average}$ versus $w_{c,average}$ and (b) $\eta_{average}$ versus $w_{c,max}$.

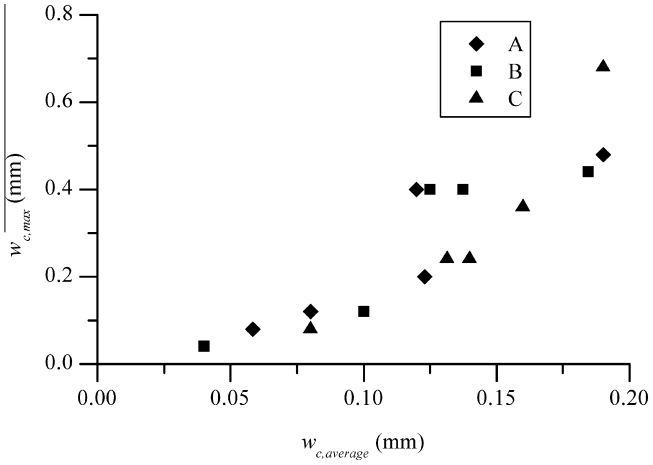

Fig. 10. The relationship between the average crack width and the maximum crack width.

3. Results and discussion

3.1. Corrosion-induced cracking analysis

For one location of the beam, the sum of crack widths on the two beam surfaces located in the same corroded area of one bar was calculated. Fig. 5 graphically shows an example of two crack configurations, in which configuration one has an equivalent width w_{eq} corresponding to the sum of the width of two cracks, while configuration two has an equivalent width w_{eq} corresponding to the width of only one crack. This kind of equivalent crack widths was previously used by Vidal et al. [22].

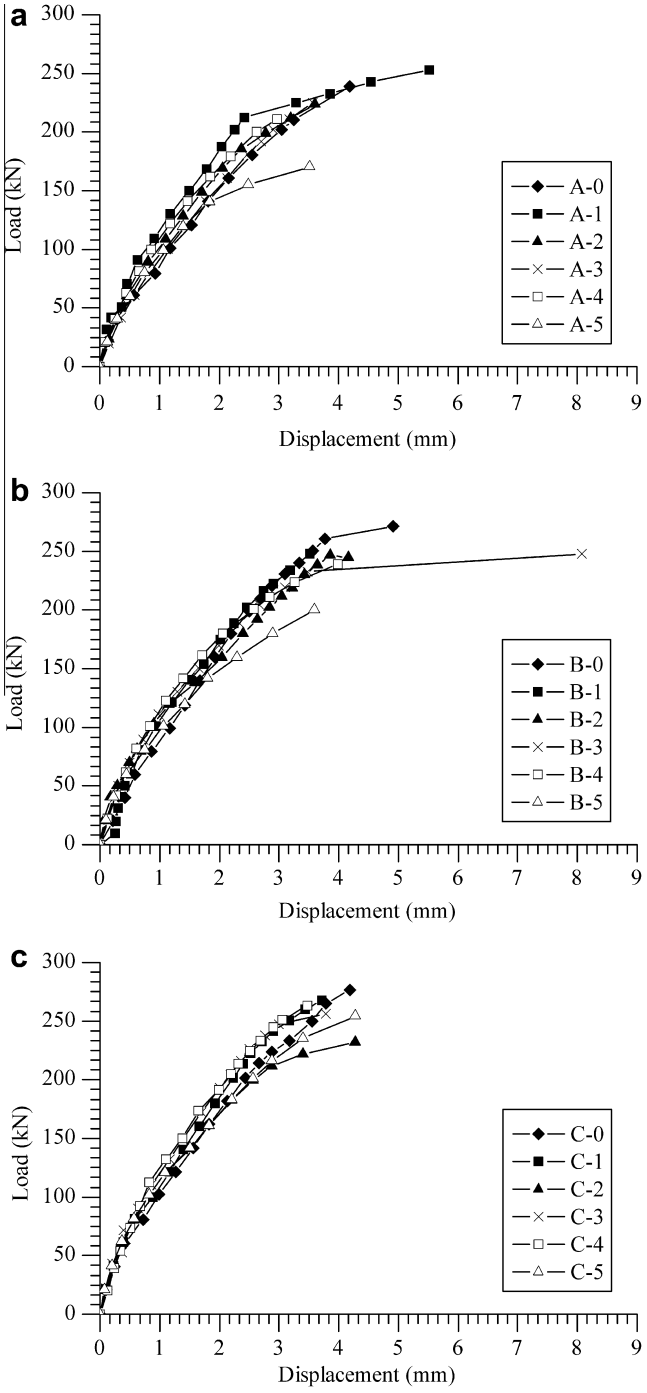

Fig. 11. Experimentally obtained load–displacement response curves. (a) Series A; (b) Series B and (c) Series C.

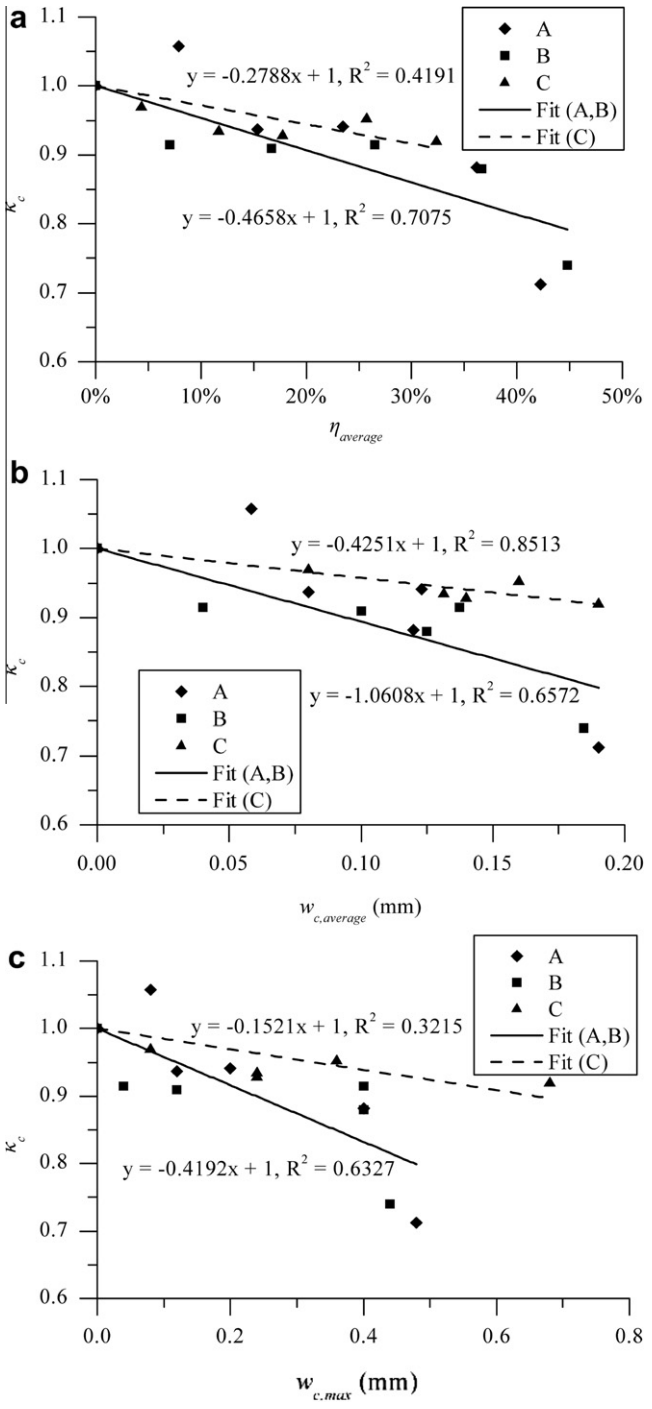

Fig. 12. Deterioration curves of the relative shear capacity of the tested beams. (a) $\eta_{average}$ versus κ_v; (b) $w_{c,averge}$ versus κ_v and (c) $w_{c,max}$ versus κ_v.

Table 4
Proposed equations for calculating κ_v.

Parameter	κ_v	Coefficient of determination (R^2)
(a) Stirrup diameter: 6 mm.		
$\eta_{average}$	$1-0.466\eta_{average}$	0.708
$w_{c,average}$	$1-1.034w_{c,average}$	0.614
$w_{c,max}$	$1-0.419w_{c,max}$	0.633
(b) Stirrup diameter: 8 mm		
$\eta_{average}$	$1-0.279\eta_{average}$	0.419
$w_{c,average}$	$1-0.408w_{c,average}$	0.829
$w_{c,max}$	$1-0.152w_{c,max}$	0.363

Using the method shown in Fig. 3a, surface crack maps were obtained for each of the tested beams and are plotted here in Figs. 6–8 for beams in groups A, B and C, respectively. Crack distribution and crack width (numbered in mm unit) at each grid of the corrosion zone are drawn on the maps. According to the above assumption, the average crack width $w_{c,average}$ and maximum crack width $w_{c,max}$ for each of the tested beams were also calculated and the corresponding results are given in Table 3.

Fig. 9 shows the relationships between the average cross-section loss ratio of the stirrup bars and the average and maximum crack widths of the concrete cover. Although the data are somewhat scatter the figure does show that both the average and maximum crack widths increase with the average cross-section loss ratio. This finding is similar to that previously reported by Vidal et al. [22] for the cracks induced by the longitudinal reinforcing steel bars. It can be seen from Fig. 9 that, beams in groups A and B have the similar feature; while beams in group C seems somewhat different from them. This is probably due to the number of stirrups and the bar diameter used in the stirrups that are different in beams in group C from beams in groups A and B. In literature, great attempt has been made in developing models to predict the cracks of concrete cover induced by the reinforcing steel corrosion [23–27]. However, most of them were for the cracks induced only by the corrosion of longitudinal reinforcing steel bars. In the present experiments, the cracks in concrete cover were induced mainly by the corrosion of stirrups although minor corrosion of longitudinal reinforcing bars was also observed in the tests as they were connected to the stirrups during the accelerated wetting–drying cycle process.

Besides the cross-section loss and the reinforcing steel bar diameter, the cover depth will also affect the corrosion-induced crack width. Generally, the initial cross-section loss, which is able to induce concrete cover cracking, increases with the cover depth, but decreases with the reinforcing steel bar diameter. In another words, with the same cross-section loss, the smaller the steel bar diameter or the larger the cover depth, the smaller the corrosion-induced crack width. However, on the other hand, since the measurement of the crack width was taken on the surface of the concrete, the thicker the concrete cover, the larger the crack width will be measured [19]. Therefore, the cover depth has a two contradicting effects on the corrosion-induced crack width, and should be considered serious for different situations.

Fig. 10 shows the relationships between the maximum crack width and the average crack width for all beams in the three groups. The figure shows that the maximum crack width increases with the average crack width. Most beams in the three groups exhibit a similar nonlinear increasing tendency. It is interesting to notice from Fig. 10 that, as the corrosion becoming more and more severe, the maximum crack width increases more rapidly with the average crack width. This is probably due to the localised stresses developed after a certain degree of cracking was formed. As cracks can stop the transfer of stresses from one place to another, when the concrete has mature cracks the stresses generated at a particular area cannot completely spread out. Therefore the cracks within the stressed area will develop quickly, whereas the cracks in isolated areas will remain unchanged.

3.2. Residual shear capacity of the corroded beams

Fig. 11 shows the load–displacement responses of the tested beams of different corroded levels in which the load is the total load recorded at the hydraulic loading point and the displacement is the deflection of the beam at the central point. It can be seen from the figure that, when the load is very small, the corroded and un-corroded beams have almost no difference in the load–displacement curves. However, when the load increased beyond 20–

30% of its ultimate load, the difference becomes clear and the corroded beams have higher deflection than the corresponding un-corroded beams for the same load level. The ultimate shear strength for each tested beam, V_u, is provided collectively in Table 3. The results show that, for the same corrosion lever the beams in groups B and C, which have high longitudinal reinforcing steel bar ratio, have higher shear capacity than the beams in group A, which have low longitudinal reinforcing steel bar ratio.

Let κ_v be the relative shear capacity of the beam, which is defined as the ratio of the shear capacity of the corroded beam to that of the un-corroded beam as follows:

$$\kappa_v = \frac{V_{uc}}{V_{u0}} \tag{3}$$

where V_{uc} is the shear capacity of the corroded beam and V_{u0} is the shear capacity of the corresponding un-corroded beam. Since the average cross-section loss ratio reflects the deterioration of the reinforcing steel bars in stirrups and the average and maximum crack widths represent the damage of concrete cover as the consequence of the corrosion of the reinforcing steel bars, both of them can be linked to the shear capacity of the beam. Note that the average cross-section loss of reinforcing steel bars in real structures is very difficult to obtain and there is no non-destructive method available at present for determining this parameter. Hence, to use the average or the maximum crack width, instead of the average cross-section loss of the reinforcing steel bars, to represent the shear capacity reduction can overcome some difficulties. With the assumption that only cracks (no delamination) are present due to corrosion, possible correlations between the average or maximum crack width and the relative shear capacity of the beam may be discovered. Fig. 12 shows the variation of the relative shear capacity with the average cross-section loss ratio (Fig. 12a), the average crack width (Fig. 12b), and the maximum crack width (Fig. 12c). It can be seen from these figures that, the reductions of the relative shear capacity with these three parameters are very similar although the reduction rates are different. Since the shear capacity

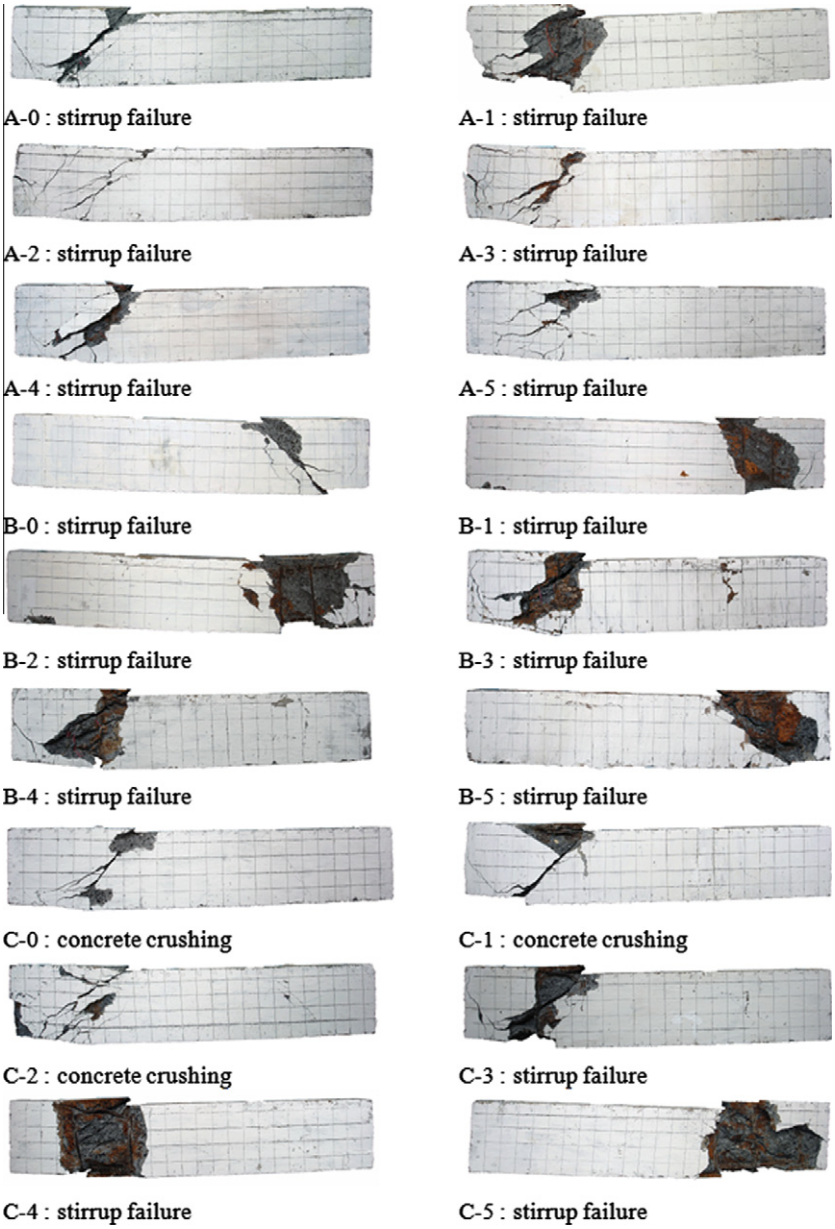

Fig. 13. Failure patterns of the tested beams.

is mainly controlled by the stirrup corrosion, the correlation lines are deduced according to the diameter of the stirrup bars, in which case groups A and B having an identical stirrup bars share in one case and group C having different stirrup bars is in the other. The deducted line fits shown in Fig. 12 indicate that, overall, the average crack width has the best correlation with the relative shear capacity, while the correlation of the maximum crack width and the average cross-section loss ratio with the relative shear capacity are similar. This implies that the relative shear capacity can be estimated if the average crack width or the maximum crack width can be obtained in a corroded beam. For a field structure, crack widths can be measured with reasonable accuracy with no difficulty and therefore the residual shear strength of the corroded beam can be estimated using the proposed correlation equations provided in Table 4 and shown in Fig. 12.

3.3. Failure modes

As all longitudinal reinforcing steel bars were well anchored at the two ends of the tested beam, no premature slip of bars occurred and the longitudinal reinforcing steel bars provided along the length of the beam served its purpose by safeguarding against any unwanted premature flexural failure. The diagonal cracks advanced from the loading point towards the support point. Failure of the beam was assumed to occur when the applied load on the beam began to drop, while the mid-span deflection continued to increase. As is to be expected, all of the beams were failed in shear (see Fig. 13) either by concrete crushing (Fig. 14a) or by stirrup failure (Fig. 14b). All beams in groups A and B were found to fail by the stirrup failure. Beams C3, C4 and C5 were also found to fail by the stirrup failure. Only beams C-0, C-1 and C-2 were found to fail by the concrete crushing. This implies that the failure mode of a corroded beam could change from concrete crushing to stirrups failure as the corrosion of the stirrups becomes severer.

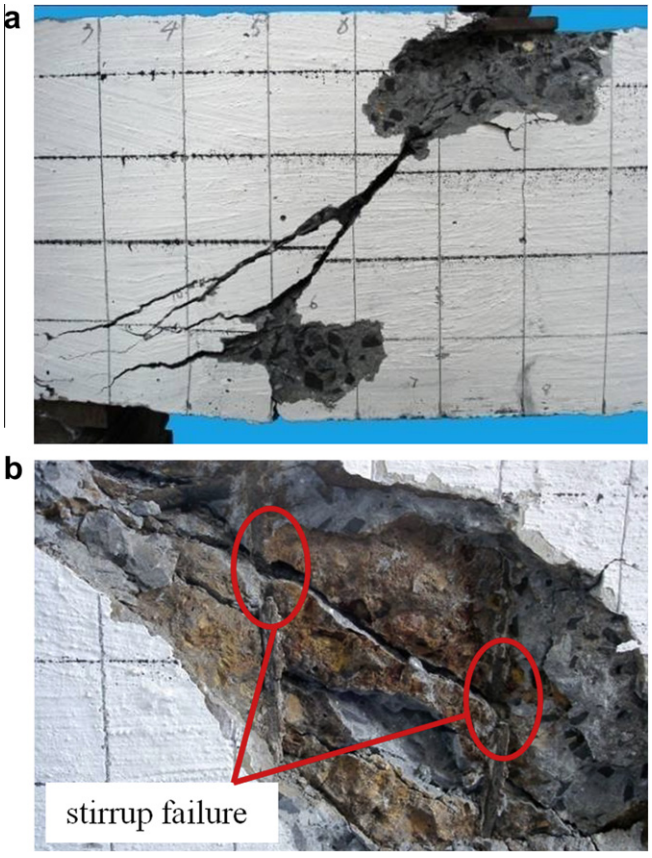

Fig. 14. Two typical failure modes observed in experiments. (a) concrete crushing and (b) stirrup failure.

4. Conclusions

Based on the results obtained from the experiments the following conclusions can be drawn:

(1) The average crack width or the maximum crack width of the concrete cover induced by the reinforcing steel corrosion can be used as an indicator of the corrosion level of the corroded reinforcing steel bars. The severer the corrosion level of the reinforcing steel bars, the wider the average crack width and so is the maximum crack width of the concrete cover. However, the development of accurate relationships between them requires more experimental data for beams with different concrete covers and different reinforcing steel bar diameters.

(2) The maximum crack width increases with the average crack width. However, the relationship between them is not linear. As the corrosion becoming more and more severe, the maximum crack width increases more quickly with the average crack width.

(3) Both the stiffness and shear capacity of the beam decrease as the corrosion level increases. However, the decrease of the stiffness is insignificant when the applied load is relatively low. It is only when the applied load exceeds 20–30% of its ultimate load, the stiffness loss caused due to the reinforcing steel corrosion becomes significant.

(4) The shear capacity of the beam decreases with the increase of the corrosion level of the corroded reinforcing steel bars or the increase of the average and maximum crack widths of the concrete cover. Among these three parameters, the average crack width was found to have the best correlation with the reduction of the shear capacity caused by the reinforcing steel corrosion.

(5) As the corrosion level becomes severer, shear failure mode of the beams may change from concrete crushing to stirrup failure. This is attributed to the cross-section loss of stirrup bars, which becomes severer as the corrosion level increases.

Acknowledgements

This work was supported by The Royal Society through an international joint project (JP0867232) and The National Natural Science Foundation of China through an international key project (50920105806).

References

[1] A.A. Almusallam, Effect of degree of corrosion on the properties of reinforcing steel bars, Construct. Build. Mater. 15 (2001) 361–368.
[2] K.Y. Ann, H.W. Song, Chloride threshold level for corrosion of steel in concrete, Corros. Sci. 49 (2007) 4113–4133.
[3] Y.G. Du, L.A. Clark, A. Chan, Residual capacity of corroded reinforcing bars, Mag. Concr. Res. 57 (2005) 135–147.
[4] A. Garces, M.C. Andrade, A. Saez, M.C. Alonso, Corrosion of reinforcing steel in neutral and acid solutions simulating the electrolytic environments in the micropores of concrete in the propagation period, Corros. Sci. 47 (2005) 289–306.
[5] A.K. Azad, S. Ahmad, S.A. Azher, Residual strength of corrosion-damaged reinforced concrete beams, ACI Mater. J. 104 (2007) 40–47.
[6] A.A. Torres-Acosta, S. Navarro-Gutierrez, J. Teran-Guillen, Residual flexure capacity of corroded reinforced concrete beams, Eng. Struct. 29 (2007) 1145–1152.
[7] C. Higgins, W.C. Farrow, Tests of reinforced concrete beams with corrosion-damaged stirrups, ACI Struct. J. 103 (2006) 133–141.

[8] W.L. Jin, F. Yan, L. Zhang, A predeterminate model of steel bar corrosion ratio considered of concrete carbonation model, J. Zhejiang Univ. (Eng. Sci.) 34 (2000) 158–163.
[9] J. Cairns, Strength in shear of concrete beams with exposed reinforcement, Proceedings of the Institution of Civil Engineers, Structures and Buildings 110 (1995) 176–185.
[10] J. Rodriguez, L.M. Ortega, J. Casal, Load carrying capacity of concrete structures with corroded reinforcement, Constr. Build. Mater. 11 (1997) 239–248.
[11] X.K. Yan, T.C. Wang, Y.M. Zhang, Shear strength of reinforced concrete beams under sea water, Trans. Tianjin Univ. 10 (2004) 138–141.
[12] S.H. Xu, D.T. Niu, The shear behavior of corroded simply supported reinforced concrete beam, J. Build. Struct. 25 (2004) 98–104.
[13] Y.X. Zhao, J. Chen, W.L. Jin, Design of shear strengths of corroded reinforced concrete beams, Int. J. Model. Identif. Control 7 (2009) 190–198.
[14] Y.S. Yuan, Y.S. Ji, S.P. Shah, Comparison of two accelerated corrosion techniques for concrete structures, ACI Struct. J. 104 (2007) 344–347.
[15] Y.S. Yuan, Y.S. Ji, Development of corrosion layer of steel bar in concrete and its mechanical and electrochemical effects, Int. J. Struct. Eng. 1 (2010) 199–206.
[16] F. Zhang, J.S. Pan, C.J. Lin, Localized corrosion behaviour of reinforcement steel in simulated concrete pore solution, Corros. Sci. 51 (2009) 2130–2138.
[17] L.Y. Li, C.L. Page, Finite element modelling of chloride removal from concrete by an electrochemical method, Corros. Sci. 42 (2000) 2145–2165.
[18] T. Luping, L.O. Nilsson, Rapid determination of the chloride diffusivity in concrete by applying an electric field, ACI Mater. J. 89 (1993) 49–53.
[19] J. Wei, X.W. Zhou, K.Q. Zhang, P. Li, Correlation analysis of durability and concrete cover thickness of concrete structure, Int. J. Struct. Eng. 1 (2008) 207–214.
[20] ASTM G102–89. Practice for calculation of corrosion rates and related information from electrochemical measurements, ASTM West Conshohocken, PA, 1999.
[21] ASTM G1–03. Standard practice for preparing, cleaning, and evaluating corrosion test specimens, ASTM West Conshohocken, PA, 2003.
[22] T. Vidal, A. Castel, R. Francois, Analyzing crack width to predict corrosion in reinforced concrete, Cement Concr. Res. 34 (2004) 165–174.
[23] H.S. Wong, Y.X. Zhao, A.R. Karimi, N.R. Buenfeld, W.L. Jin, On the penetration of corrosion products from reinforcing steel into concrete due to chloride-induced corrosion, Corros. Sci. 52 (2010) 2469–2480.
[24] R. Zhang, A. Castel, R. Fran Ois, Concrete cover cracking with reinforcement corrosion of RC beam during chloride-induced corrosion process, Cement Concr. Res. 40 (2010) 415–425.
[25] L. Chernin, D.V. Val, Prediction of corrosion-induced cover cracking in reinforced concrete structures, Construct. Build. Mater. 25 (2010) 1854–1869.
[26] K. Bhargava, A.K. Ghosh, Y. Mori, S. Ramanujam, Model for cover cracking due to rebar corrosion in RC structures, Eng. Struct. 28 (2006) 1093–1109.
[27] G. Malumbela, M. Alexander, P. Moyo, Model for cover cracking of RC beams due to partial surface steel corrosion, Construct. Build. Mater. 25 (2011) 987–991.